

# No-Reference Image Quality Assessment by Hallucinating Pristine Features

Baoliang Chen, Lingyu Zhu, Chenqi Kong, Hanwei Zhu, Shiqi Wang, *Member, IEEE* and Zhu Li, *Senior Member, IEEE*

**Abstract**—In this paper, we propose a no-reference (NR) image quality assessment (IQA) method via feature level pseudo-reference (PR) hallucination. The proposed quality assessment framework is grounded on the prior models of natural image statistical behaviors, and rooted in the view that the perceptually meaningful features could be well exploited to characterize the visual quality. Herein, the PR features from the distorted images are learned by a mutual learning scheme with the pristine reference as the supervision, and the discriminative characteristics of PR features are further ensured with the triplet constraints. Given a distorted image for quality inference, the feature level disentanglement is performed with an invertible neural layer for final quality prediction, leading to the PR and the corresponding distortion features for comparison. The effectiveness of our proposed method is demonstrated on four popular IQA databases, and superior performance on cross-database evaluation also reveals the high generalization capability of our method. The implementation of our method is publicly available on <https://github.com/Baoliang93/FPR>.

**Index Terms**—Image quality assessment, no-reference, mutual learning, pseudo-reference feature

## I. INTRODUCTION

IMAGE quality assessment (IQA), which aims to establish the quantitative connection between the input image and the corresponding perceptual quality, serves as a key component in a wide range of computer vision applications [1], [2], [3]. The typical full-reference (FR) IQA models resort to the fidelity measurement in predicting image quality via measuring the deviation from its pristine-quality counterpart (reference). The pioneering studies date back to 1970's and a series of visual fidelity measures have been investigated [4]. Recently, there has been a demonstrated success for developing the FR quality measures, including the Peak Signal-to-Noise Ratio (PSNR), Structural Similarity Index (SSIM) [5], Multiscale SSIM (MS-SSIM) [6], Visual Saliency-Induced Index (VSI) [7], Median Absolute Deviation (MAD) [8] and Visual Information Fidelity (VIF) [9]. Unfortunately, in the vast majority of practical applications, the reference images are usually absent or difficult to obtain, leading to the exponential increase in the demand for no-reference (NR) IQA methods. Comparing with FR-IQA, NR-IQA is a more challenge task due to the lack of pristine reference information.

B. Chen, L. Zhu, C. Kong, H. Zhu and S. Wang are with the Department of Computer Science, City University of Hong Kong, Hong Kong (e-mail: blchen6-c@my.cityu.edu.hk; lingyuzhu-c@my.cityu.edu.hk; cqkong2-c@my.cityu.edu.hk; hzwu4-c@my.cityu.edu.hk; shiqwang@cityu.edu.hk).

Z. Li is with the Department of Computer Science and Electrical Engineering, University of Missouri-Kansas City, MO 64110, USA. (email:zhu.li@ieee.org).

In the literature, numerous NR-IQA methods have been proposed based on the hypothesis that natural scenes possess certain statistical properties. Thus, the quality can be assessed by measuring the deviation of the statistics between distorted and pristine images [10], [11], [12]. With the development of deep learning technologies, the image quality can be inferred by learning from the labeled image data [13], [14], [15], [16], [17], [18], [19]. However, such data driven based methods highly rely on the large-scale training samples. Recently, the free energy based brain theory [20], [21], [22], [23] provides a novel solution for NR-IQA from the Bayesian view. In particular, the free energy theory reveals that human visual system (HVS) always attempts to reduce the uncertainty and explains the scene of perceived visual stimulus by an internal generative model. Rooted in the widely accepted view that the intrinsic, perceptually-meaningful and learnable features could govern the image quality, in this work we focus on the generative model at the feature level for NR-IQA. This method avoids the modeling of the image signal space of which the understanding is still quite limited. Herein, we propose to learn a new NR-IQA measure named **FPR**, by inferring the quality through Feature-level **PR** information. The underlying design philosophy of our method is learning the quality-specific PR feature instead of the restoration-specific PR feature. Along this vein, we can get rid of the design of a specific network for PR image generation, which is still a very challenging task. To verify the performance of our method, we conduct both intra-database and cross-database experiments on four databases, including TID2013 [24], LIVE [25], CSIQ [8] and KADID-10k [26]. Experimental results have demonstrated the superior performance of our method over existing state-of-the-art models. The main contributions of this paper are summarized as follows,

- We propose a novel NR-IQA framework based on the PR information constructed at the feature-level. This scheme aims to infer the pristine features that enjoy the advantages of quality-aware, learnable and discriminative.
- We learn the PR feature by a mutual learning strategy, leveraging the reference information. To improve the discrimination capability between the estimated PR feature and the distortion feature, a triplet loss is further adopted.
- We develop the aggregation strategy for the predicted scores of different patches in an image. The strategy benefits from the gated recurrent units (GRU), and generates the attention map of the testing image for quality aggregation.

## II. RELATED WORKS

Due to the lack of reference information, the existing NR-IQA measures can be classified into two categories: quality-aware feature extraction based NR-IQA and discrepancy estimation based NR-IQA. In the first category, the quality-aware features are extracted based on a NSS model or a data-driven model, and the quality is finally predicted by a regression module. In the second category, the PR image/images are first constructed, then the discrepancy between the input image and its PR image/images are measured. The philosophy is that the larger the discrepancy, the worse quality the image possesses. Herein, we provide an overview of the two categories of NR-IQA models as well as the mutual learning methods.

### A. Quality-Aware Feature Extraction based NR-IQA

Typically, conventional NR-IQA methods extract the quality-aware features based on the natural scene statistics (NSS) and predict the image quality by evaluating the destruction of naturalness. In [27], [28], based on the Mean-Subtracted Contrast-Normalized (MSCN) coefficients, the NSS are modeled with a generalized Gaussian distribution and the quality can be estimated by the distribution discrepancy. The NSS features have also been exploited in the wavelet domain, [29], [12], [30], [31]. In [30], to discriminate degraded and undegraded images, the complex pyramid wavelet transform is performed and the magnitudes and phases of the wavelet coefficients are characterized as the NSS descriptor. Analogously, in [11], the discrete cosine transform (DCT) is introduced for NSS model construction, leading to a Bayesian inference based NR-IQA model. Considering the structural information is highly quality-relevant, the joint statistics of gradient magnitude and Laplacian of Gaussian response are utilized in [32] to model the statistical naturalness. In [33], the hybrid features consisting of texture components, structure information and intra-predicted modes are extracted and unified for adaptive bitrate estimation. Recently, there has been a surge interest in deep-feature extraction for NR-IQA. In [13], a shallow ConvNet is first utilized for the patch-based NR-IQA learning. This work is extended by DeepBIQ [16], where a pre-trained convolutional neural network (CNN) is fine-tuned for the generic image description. Instead of learning only from the quality score, the multi-task CNN was proposed in [34], in which both the quality estimation and distortion identification are learned simultaneously for the better quality degradation measure. However, although those deep-learning based methods have achieved high performance improvement, the insufficient training data usually create the over-fitting problem. To alleviate this issue, extra synthetic databases *e.g.* [35], [36], [37] have been proposed for more generalized model learning. The training data can also be enriched by ranking learning. In [38], [39], [40], [37], the quality scores of an image pair are regressed and ranked, leading to the more quality-sensitive feature extraction.

### B. Discrepancy Estimation based NR-IQA

The NR-IQA problem can be feasibly converted to the FR-IQA problem when the reference image can be inferred

through generative models. In [41], the PR image is generated by a quality-aware generative network, then the discrepancy between the distorted image and PR image are measured for quality regression. In contrary to constructing the PR image with perfect quality, the reference information provided by the PR image that suffered from the severest distortion was explored in [42], then an NR-IQA metric was developed by measuring the similarity between the structures of distorted and the PR images. In [43], both a pristine reference image (generated via a restoration model) and a severely distorted image (generated via a degradation model) are utilized for quality prediction. Analogously, through comparing the distorted images and its two bidirectional PRs, the bilateral distance (error) maps are extracted in [44].

### C. Mutual Learning

The assumption of mutual learning is highly relevant with the dual learning and collaborative learning, as their assumptions all lie in the encouragement of the models to teach each other during training. For example, the dual learning was adopted in [45], where two cross-lingual translation models are forced to learn from each other through the reinforcement learning. Comparing with dual learning, the same task is learned in the collaborative learning. In [46], multiple student models are expected to learn the same classification task while their inputs are sampled from different domains. Different from the dual learning and collaborative learning, both the tasks and inputs of the models in mutual learning are identical. For example, the deep mutual learning was utilized in [47], where two student models are forced to learn the classification collaboratively by a Kullback Leibler (KL) loss. This work was further extended in [48], with the KL loss replaced by a generative adversarial network. In our method, the mutual learning strategy was adopted to improve the learnability of the PR feature and we further impose the triplet constraint to the output features, significantly enhancing their discriminability.

## III. THE PROPOSED SCHEME

We aim to learn an NR-IQA measure by hallucinating the PR features. In the training stage, given the pristine reference, we attempt to build a FR-IQA model with the distorted and corresponding pristine reference images. The PR feature is subsequently learned in a mutual way. Finally, the GRU based quality aggregation is performed to obtain the final quality score.

### A. PR Feature Learning

As shown in Fig. 1, in the training phase, we learn to hallucinate the PR feature  $F^{PR}$  from a single distorted image by the guidance of the pristine reference feature  $F^R$ . In particular, the  $F^R$  is generated from a FR model based on the quality-embedding feature extractor and the  $F^{PR}$  is decomposed from the feature  $F^{NR}$  which is regarded as a fusion feature that contains the entire information of the PR feature  $F^{PR}$  and the distortion feature  $F^D$ .

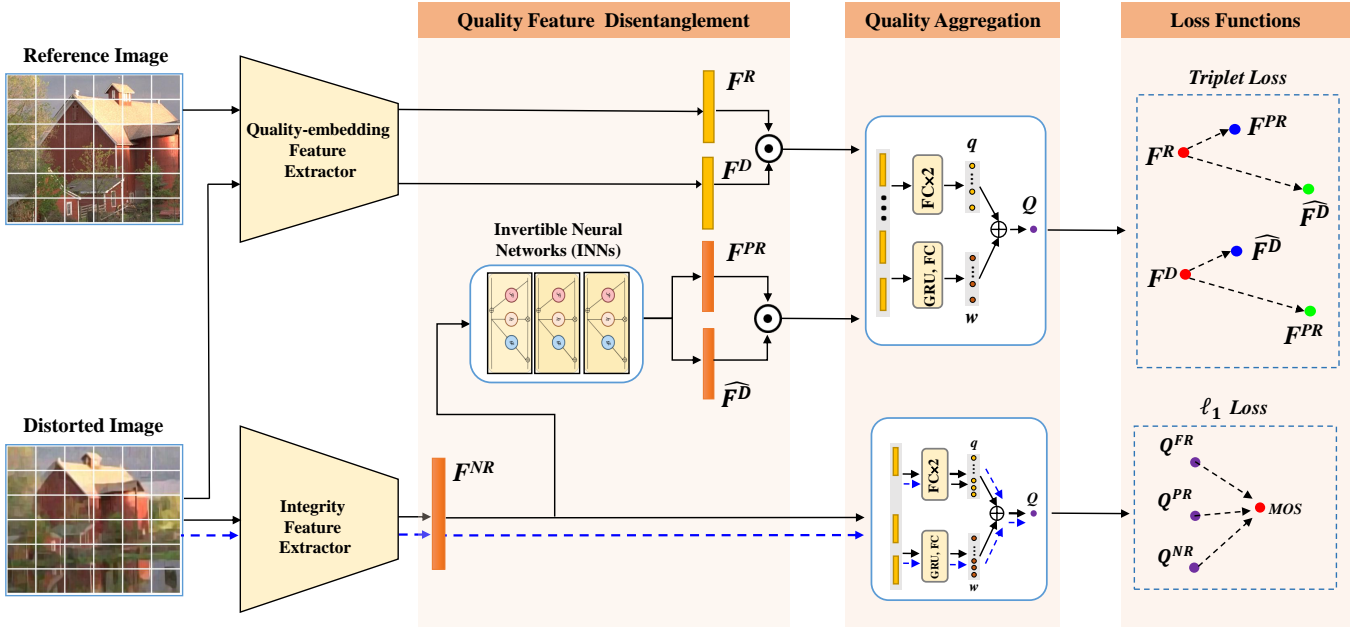


Fig. 1. The framework of our proposed method. Two feature extractors are utilized in the training phase: the quality-embedding feature extractor and the integrity feature extractor. For the quality-embedding feature extractor, we extract the quality-embedding features  $F^D$  and  $F^R$  from the distortion image and its reference image, respectively. For the integrity feature extractor, we aim to extract the feature  $F^{NR}$  from a single distorted image that contains the fusion information of a PR feature  $F^{PR}$  and a distortion feature  $\hat{F}^D$  by the guidance of  $F^R$  and  $F^D$ . Then the quality of the distorted image can be regressed by the  $F^{NR}$ . Finally, we further propose a GRU based quality aggregation module for patch-wise quality score aggregation. In the testing phase, only the testing image (without reference) is available for quality prediction based on the proposed NR-IQA model.

In general, there are two properties a desired PR feature should possess. First, the PR feature should be learnable. Generally speaking, it is an ill-posed problem for learning the PR information from the distorted image. Though in the training process the reference image could be taken advantage of, the PR feature may not be able to be feasibly learned by only forcing the inferred PR feature to be close to the feature of the reference image. As such, the learning capability of the NR-IQA network should be carefully considered during the reference feature generation. Second, the PR feature should be discriminative enough when comparing with the distortion feature. Enhancing the discriminability could improve the quality sensitivity of the PR feature and subsequently promote the prediction performance.

The proposed method is conceptually appealing in the sense of learnability and discriminability. Regarding the learnability, a mutual learning strategy is adopted. As shown in Fig. 1, in the training process, the paired images including the distorted image and its corresponding reference are fed into the quality-embedding feature extractor, generating the reference feature  $F^R$  and distortion feature  $F^D$ . The integrity feature extractor, which accepts the distorted image only, is encouraged to generate the feature  $F^{NR}$  that contains the full information of the pseudo reference feature  $F^{PR}$  and the distortion feature  $\hat{F}^D$ . The mutual learning strategy enables the integrity feature extractor and quality-embedding feature extractor to be learned simultaneously with the feature distance constraint. Thus,

more learnable reference feature can be generated by the FR model. The connection among the features  $F^{NR}$ ,  $F^{PR}$  and  $\hat{F}^D$  are constructed by an invertible layer, consisting of three invertible neural networks (INNs). Through the INNs, the integrity feature  $F^{NR}$  can be disentangled into a pseudo reference feature  $F^{PR}$  and a distortion feature  $\hat{F}^D$ , without losing any information due to the invertibility of INNs.

To equip the discriminative capability, a triplet loss is further utilized [49] as the distance measure between the reference features ( $F^R$ ,  $F^{PR}$ ) and the corresponding distortion features ( $F^D$  and  $\hat{F}^D$ ), which is expressed as follows,

$$\mathcal{L}_{trip} = \sum_{i=1}^N \left[ \|F_i^R - F_i^{PR}\|_2^2 - \|F_i^R - \hat{F}_i^D\|_2^2 + \alpha \right]_+ + \sum_{i=1}^N \left[ \|\hat{F}_i^D - \hat{F}_i^D\|_2^2 - \|\hat{F}_i^D - F_i^{PR}\|_2^2 + \alpha \right]_+, \quad (1)$$

where  $i$  is input patch index in a batch,  $N$  is the batch size and  $\alpha$  is a margin that is enforced between positive and negative pairs. With this loss, on the one hand, the distance between the reference feature and PR feature can be reduced. On the other hand, the discrepancies between the reference/PR feature and two distortion features can be enlarged.

As illustrated in Fig. 1, to maintain the relationship of  $F^{PR}$  and  $\hat{F}^D$  to be consistent with  $F^R$  and  $F^D$ , we concatenate  $F^R$  with  $F^D$  (denoted as  $Concat(F^R, F^D)$ ) and  $F^{PR}$  with  $\hat{F}^D$

(denoted as  $Concat(F^{PR}, \hat{F}^D)$ ) for quality prediction through a shared quality aggregation module.

### B. GRU Based Quality Aggregation

To aggregate the predicted quality score of each patch in an image, the aggregation module should be invariant of the patch numbers. In this paper, we propose a GRU based quality score aggregation module as shown in Fig. 1. More specifically, regarding the concatenated features  $Concat(F^R, F^D)$  and  $Concat(F^{PR}, \hat{F}^D)$ , two sub-branches are adopted for quality prediction. The first branch is a fully-connected (FC) layer which is responsible for patch-wise quality prediction with the patch-wise concatenated feature as input. Another sub-branch consists of one GRU layer and one FC layer. Different from [15], the inputs of the GRU layer are the features of all the patches in an image. With GRU, the long-term dependencies between different patches can be modeled and synthesized, then we normalize the output weights from the last FC layer for final attention map generation,

$$w_i = \frac{\alpha_i}{\sum_{j=1}^{N_p} \alpha_j}, \quad (2)$$

where  $i$  is patch index in an image,  $N_p$  is the number of patches and  $p_i$  is the attention weight of  $i$ -th patch. Finally, the global image quality  $Q$  can be estimated as

$$Q = \sum_{i=1}^{N_p} w_i q_i = \frac{\sum_{i=1}^{N_p} \alpha_i q_i}{\sum_{i=1}^{N_p} \alpha_i}, \quad (3)$$

where  $q_i$  is the predicted quality of  $i$ -th patch. As shown in Fig. 1, we also adopt the same strategy (network) for the quality aggregation of the patch-wise integrity feature  $F^{NR}$ . Due to the distinct representations of the fused feature and concatenated features, the parameters of the two aggregation modules are not shared during the model training.

### C. Objective Function

In summary, the objective function in our proposed method include two triplet losses and three quality regression losses. In particular, for quality regression, comparing with mean squared error (MSE), optimization with mean absolute error (MAE) is less sensitive to the outliers, leading to a more stable training processing. Consequently, the objective function is given by,

$$\begin{aligned} \mathcal{L} &= \mathcal{L}_{mse} + \lambda \mathcal{L}_{trip} \\ &= \sum_{j=1}^{N_I} \left[ \left| \hat{Q}_j - Q_j^{FR} \right| + \left| \hat{Q}_j - Q_j^{PR} \right| + \left| \hat{Q}_j - Q_j^{NR} \right| \right] \\ &\quad + \lambda \left( \sum_{i=1}^{N_I * N_P} \left[ \left\| F_i^R - F_i^{PR} \right\|_2^2 - \left\| F_i^R - \hat{F}_i^D \right\|_2^2 + \alpha \right]_+ \right) \\ &\quad + \lambda \left( \sum_{i=1}^{N_I * N_P} \left[ \left\| F_i^D - \hat{F}_i^D \right\|_2^2 - \left\| F_i^D - F_i^{PR} \right\|_2^2 + \alpha \right]_+ \right), \end{aligned} \quad (4)$$

where  $i$  and  $j$  are the patch index and image index, respectively.  $N_I$  is the number of images in a batch and  $\hat{Q}_j$

is the Mean Opinion Score (MOS) provided by the training set.  $Q^{FR}$ ,  $Q^{PR}$ ,  $Q^{NR}$  are the quality scores predicted from the features  $Concat(F^R, F^D)$ ,  $Concat(F^{PR}, \hat{F}^D)$  and  $F^{NR}$ , respectively. It is also worth noting that the extractions of  $F^R, F^D, F^{PR}, \hat{F}^D$  are not necessary in the testing phase, and we only adopt the  $Q^{NR}$  for the final quality prediction, thus the computational complexity in testing phase can be highly reduced comparing with the network used in the training phase.

## IV. EXPERIMENTAL RESULTS

1) *IQA Databases*: Since our model is trained in a paired manner, the reference image should be available during the training phase. As such, to validate the proposed method, we evaluate our model on four synthetic IQA databases including: TID2013 [24], LIVE [50], CSIQ [8] and KADID-10k [26]. More details are provided in Table I.

**TID2013.** The TID2013 database consists of 3,000 images obtained from 25 pristine images for reference. The pristine images are corrupted by 24 distortion types and each distortion type corresponds to 5 levels. The image quality is finally rated by double stimulus procedure and the MOS values are obtained in the range [0, 9], where larger MOS indicates better visual quality.

**LIVE.** The LIVE IQA database includes 982 distorted natural images and 29 reference images. Five different distortion types are included: JPEG and JPEG2000 compression, additive white Gaussian noise (WN), Gaussian blur (BLUR), and Rayleigh fast-fading channel distortion (FF). Different from the construction of TID2013, a single-stimulus rating procedure is adopted for quality rating, producing a range of difference mean opinion scores (DMOS) from 0 to 100 and a lower DMOS value represents better image quality.

**CSIQ.** The CISQ database contains 30 reference images and 866 distorted images. This database involves six distortion types: JPEG compression, JP2K compression, Gaussian blur, Gaussian white noise, Gaussian pink noise and contrast change. The images are rated by 35 different observers and the DMOS results are normalized into the range [0, 1].

**KADID-10k.** In this database, 81 pristine images are included and each pristine image is degraded by 25 distortion types in 5 levels. All the images are resized into the same resolution (512×384). For each distorted image, 30 reliable degradation category ratings have been obtained by crowdsourcing.

2) *Implementation Details*: We implement our model by PyTorch [51]. In Fig. 2, we show the layer-wise network design of our proposed method. We crop the image patches without overlapping and the size is set by 64×64. The number of image pairs in a batch is set by 32. We adopt Adam optimizer [52] for optimization. The learning rate is fixed to 1e-4 with a weight decay set as 1e-4. The weighting parameters  $\lambda, \alpha$  in Eqn. (4) are set as 20.0 and 2.0, respectively. We duplicate the samples by 16 times in a batch to augment the data. The maximum epoch is set by 1,000.

It should be mentioned that all the experimental pre-settings are fixed both in intra-database and cross-database training.

TABLE I  
DESCRIPTIONS OF THE FOUR IQA DATABASES.

Database	# of Ref. Images	# of Images	Distortion Types
TID2013 [24]	25	3,000	Additive Gaussian noise; Additive noise in color components; Spatially correlated noise; Masked noise; High frequency noise; Impulse noise; Quantization noise; Gaussian blur; Image denoising; JPEG compression; JPEG2000 compression; JPEG transmission errors; JPEG2000 transmission errors; Non eccentricity pattern noise; Local block-wise distortions of different intensity; Mean shift (intensity shift); Contrast change; Change of color saturation; Multiplicative Gaussian noise; Comfort noise; Lossy compression of noisy images; Image color quantization with dither; Chromatic aberrations; Sparse sampling and reconstruction
LIVE [50]	29	982	JPEG and JPEG2000 compression; Additive white; Gaussian noise; Gaussian blur; Rayleigh fast-fading channel distortion
CSIQ [8]	30	866	JPEG compression; JP2K compression; Gaussian blur; Gaussian white noise; Gaussian pink noise and contrast change
KADID-10k [26]	81	10,125	Blurs (Gaussian, lens,motion); Color related (diffusion, shifting, quantization, over-saturation and desaturation); Compression (JPEG2000, JPEG); Noise related (white, white with color, impulse, multiplicative white noise + denoise); Brightness changes (brighten, darken, shifting the mean); Spatial distortions (jitter, non-eccentricity patch, pixelate, quantization, color blocking); Sharpness and Contrast.

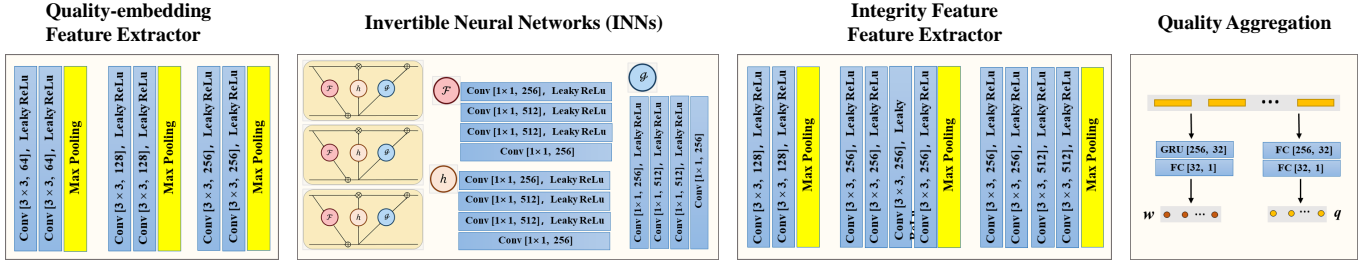


Fig. 2. Illustration of the network architectures for the quality-embedding feature extractor, INNs, integrity feature extractor and quality aggregation module.

For the intra-database evaluation, we randomly spilt the dataset into training set, validation set and testing set by reference image to guarantee there is no content overlap among the three sets. In particular, 60%, 20%, 20% images are used for training, validation and testing, respectively. We discard the 25th reference image and the distorted versions in TID2013, as they are not natural image. The experimental results on intra-database are reported based on 10 random splits. To make errors and gradients comparable for different databases, we linearly map the MOS/DMOS ranges of other three databases (TID2013, CSIQ, KADID-10k) to the DMOS range [0, 100] which is the same as LIVE database. Two evaluation metrics are reported for each experimental setting, including: Spearman rank correlation coefficient (SRCC), Pearson linear correlation coefficient (PLCC). The PLCC evaluates the prediction accuracy and the SRCC indicates the prediction monotonicity.

#### A. Quality Prediction on Intra-database

1) *Overall Performance on Individual Database*: In this sub-section, we compare our method with other state-of-the-art NR-IQA methods, including BRISQUE [27], M3 [32], FRIQUEE [53], CORNIA [54], DIIVIN [10], BLINDS-II [11],

TABLE II  
PERFORMANCE EVALUATION ON THE LIVE, CSIQ AND TID2013 DATABASES. THE TOP TWO RESULTS ARE HIGHLIGHTED IN BOLDFACE.

Method	LIVE		CSIQ		TID2013	
	SRCC	PLCC	SRCC	PLCC	SRCC	PLCC
BRISQUE [27]	0.939	0.935	0.746	0.829	0.604	0.694
M3 [32]	0.951	0.950	0.795	0.839	0.689	0.771
FRIQUEE [53]	0.940	0.944	0.835	0.874	0.68	0.753
CORNIA [54]	0.947	0.950	0.678	0.776	0.678	0.768
HOSA [55]	0.946	0.947	0.741	0.823	0.735	0.815
Le-CNN [13]	0.956	0.953	-	-	-	-
BIECON [14]	0.961	0.962	0.815	0.823	0.717	0.762
DIQaM-NR [15]	0.960	0.972	-	-	0.835	0.855
WaDIQaM-NR [15]	0.954	0.963	-	-	0.761	0.787
ResNet-ft [56]	0.950	0.954	0.876	0.905	0.712	0.756
IW-CNN	0.963	0.964	0.812	0.791	0.800	0.802
DB-CNN	<b>0.968</b>	<b>0.971</b>	<b>0.946</b>	<b>0.959</b>	0.816	0.865
CaHDC [57]	0.965	0.964	0.903	0.914	<b>0.862</b>	<b>0.878</b>
HyperIQA [57]	0.962	0.966	0.923	0.942	0.729	0.775
FPR	<b>0.967</b>	<b>0.968</b>	<b>0.948</b>	<b>0.956</b>	<b>0.872</b>	<b>0.887</b>
FPR (FR)	0.967	0.977	0.962	0.966	0.897	0.868

TABLE III  
PERFORMANCE EVALUATION ON THE KADID-10K DATABASE. THE TOP TWO RESULTS ARE HIGHLIGHTED IN BOLDFACE.

Method	BIQI [29]	BLIINDS-II [11]	BRISQUE [27]	CORNIA [54]	DIIVINE [10]	HOSA [55]	SSEQ [58]	InceptionResNetV2 (fine-tune) [26]	FPR	FPR (FR)
PLCC	0.460	0.559	0.554	0.580	0.532	0.653	0.463	<b>0.734</b>	<b>0.901</b>	0.940
SRCC	0.431	0.527	0.519	0.541	0.489	0.609	0.424	<b>0.731</b>	<b>0.899</b>	0.941

TABLE IV  
SRCC COMPARISON IN THREE DATABASES ON FOUR COMMON DISTORTION TYPES. THE TOP TWO RESULTS ARE HIGHLIGHTED IN BOLDFACE.

Dataset	Dist.Type	Method										FPR
		DIIVINE [10]	BLIINDS-II [11]	BRISQUE [27]	CORNIA [54]	HOSA [55]	WaDIQaM-NR [15]	DIQA [59]	BPRI (c) [42]	BPRI (p) [42]	TSPR [42]	
LIVE	WN	<b>0.988</b>	0.947	0.979	0.976	0.975	0.970	<b>0.988</b>	0.984	0.985	0.972	<b>0.987</b>
	GB	0.923	0.915	0.951	0.969	0.954	0.960	0.962	0.927	0.924	<b>0.978</b>	<b>0.979</b>
	JPEG	0.921	0.950	0.965	0.955	0.954	0.964	<b>0.976</b>	<b>0.967</b>	<b>0.967</b>	0.947	0.932
	JP2K	0.922	0.930	0.914	0.943	0.954	0.949	<b>0.961</b>	0.908	0.907	0.950	<b>0.965</b>
CSIQ	WN	0.866	0.760	0.682	0.664	0.604	0.929	0.835	0.931	<b>0.936</b>	0.910	<b>0.942</b>
	GB	0.872	0.877	0.808	0.836	0.841	<b>0.958</b>	0.870	0.904	0.900	0.908	<b>0.939</b>
	JPEG	0.800	0.899	0.846	0.869	0.733	0.921	0.931	0.918	0.930	<b>0.944</b>	<b>0.969</b>
	JP2K	0.831	0.867	0.817	0.846	0.818	0.886	<b>0.927</b>	0.863	0.862	0.896	<b>0.967</b>
TID 2013	WN	0.855	0.647	0.858	0.817	0.817	0.843	0.915	<b>0.918</b>	<b>0.918</b>	0.876	<b>0.931</b>
	GB	0.834	0.837	0.814	0.840	0.870	0.861	<b>0.912</b>	0.873	0.859	0.837	<b>0.912</b>
	JPEG	0.628	0.836	0.845	0.896	<b>0.986</b>	<b>0.931</b>	0.875	0.907	0.910	0.913	0.906
	JP2K	0.853	0.888	0.893	0.901	0.902	<b>0.932</b>	0.912	0.883	0.868	<b>0.935</b>	0.900

HOSA [55], Le-CNN [13], BIECON [14], WaDIQaM [15], ResNet-ft [56], IW-CNN [56], DB-CNN [56], CaHDC [57] and HyperIQA [60]. The comparison results are shown in Tables II and III. All our experiments are conducted under ten times random train-test splitting operations, and the median SRCC and PLCC values are reported as final statistics. From the table, we can observe that all competing models achieve comparable performance on LIVE database while the performance vary on more challenging databases: TID2013 and KADID-10k. Comparing with hand-crafted based methods like BRISQUE, FRIQUEE and CORNIA, the CNN-based methods can achieve superior performance on different databases, revealing that human-perception relevant features can be learned from the training set. Moreover, we can also find that our method achieves the best performance on TID2013, KADID-10k and CSIQ databases in terms of both SRCC and PLCC. Although our method achieves the second place on LIVE database, the results are still comparable (SRCC 0.967 v.s. 0.968) to the best model DB-CNN. Furthermore, different from DB-CNN, the external databases are not required for training by our proposed method.

As we train our model in a paired manner, the FR results can also be acquired during the testing by involving the reference image. Herein, we also provide the FR results denoted as FPR (FR) in Tables II and III. From the tables, we can observe that our FR model can achieve higher performance when compared with our NR model, as the pristine image provide more accurate reference information for quality evaluation. We also observe that the performance of our FR model is not as good as some other FR models *e.g.*, WaDIQaM-FR [15]. We believe this is reasonable, as the learning capability of our NR model must be considered simultaneously during the extraction of reference feature. Furthermore, we compare our method with two PR image based NR-IQA methods named BPRI [42] and TSPR [44]. Following the experimental setting in [44] that four shared distortion types, *i.e.*, JPEG, GB, WN and JP2K in the TID2013, LIVE and CSIQ databases are used for performance

comparison. The results are presented in Table IV. From the Table, we can observe that our method achieves the best performance on most settings and significantly outperforms them. These results reveal the effectiveness of our PR information constructed in feature level. Moreover, comparing with the method in [44] where a generative adversarial network (GAN) is utilized to restore the reference information at image-level, the light network utilized in our method can significantly reduce the inference time.

2) *Performance on Individual Distortion Type*: To further explore the behaviors of our proposed method, we present the performance on individual distortion type and compare it with several competing NR-IQA models. The results of experiments performed on TID2013 database and LIVE database are shown in Table V and Table VI, respectively. For each database, the average SRCC values of above ten settings are reported. As shown in the Table V, we can easily observe that our method can achieve the highest accuracy on most distortion types (over 60% subsets). By contrast, lower SRCC values are obtained on some specific distortion types, *e.g.*, mean shift. The reason may lie in the challenge of PR feature hallucination due to valuable information buried by the severe distortion. It is worth noting that our method achieves significant performance improvements on some noise-relevant distortion types (*e.g.*, additive Gaussian noise, masked noise) and compression-relevant distortion types (*e.g.*, JPEG compression, JPEG 2000 compression). The result is consistency with the performance on LIVE database, verifying the capacity that our model possesses in restoring the PR features from different distortion types.

#### B. Cross-Database Evaluation

To verify the generalization capability of our FPR model, we further evaluate our model on cross-database settings. We compare our method with seven NR-IQA methods, including: BRISQUE, M3, FRIQUEE, CORNIA, HOSA and two CNN-based counterparts DIQam-NR and HyperIQA. The results

TABLE V

AVERAGE SRCC RESULTS OF INDIVIDUAL DISTORTION TYPES ON TID2013 DATABASE. THE TOP TWO RESULTS ARE HIGHLIGHTED IN BOLDFACE.

SRCC	BRISQUE [27]	M3 [32]	FRIQUEE [53]	CORNIA [54]	HOSA [55]	MEON [36]	DB-CNN [56]	FPR
Additive Gaussian noise	0.711	0.766	0.730	0.692	<b>0.833</b>	0.813	0.790	<b>0.953</b>
Additive noise in color components	0.432	0.56	0.573	0.137	0.551	<b>0.722</b>	0.700	<b>0.897</b>
Spatially correlated noise	0.746	0.782	0.866	0.741	0.842	<b>0.926</b>	0.826	<b>0.967</b>
Masked noise	0.252	0.577	0.345	0.451	0.468	<b>0.728</b>	0.646	<b>0.876</b>
High frequency noise	0.842	0.900	0.847	0.815	0.897	<b>0.911</b>	0.879	<b>0.934</b>
Impulse noise	0.765	0.738	0.730	0.616	<b>0.809</b>	<b>0.901</b>	0.708	0.779
Quantization noise	0.662	0.832	0.764	0.661	0.815	<b>0.888</b>	0.825	<b>0.920</b>
Gaussian blur	0.871	<b>0.896</b>	0.881	0.850	0.883	<b>0.887</b>	0.859	0.833
Image denoising	0.612	0.709	0.839	0.764	0.854	0.797	<b>0.865</b>	<b>0.944</b>
JPEG compression	0.764	0.844	0.813	0.797	0.891	0.850	<b>0.894</b>	<b>0.923</b>
JPEG 2000 compression	0.745	0.885	0.831	0.846	<b>0.919</b>	0.891	0.916	<b>0.923</b>
JPEG transmission errors	0.301	0.375	0.498	0.694	0.73	0.746	<b>0.772</b>	<b>0.797</b>
JPEG 2000 transmission errors	0.748	0.718	0.660	0.686	0.710	0.716	<b>0.773</b>	<b>0.752</b>
Non-eccentricity pattern noise	0.269	0.173	0.076	0.200	0.242	0.116	<b>0.270</b>	<b>0.559</b>
Local block-wise distortions	0.207	<b>0.379</b>	0.032	0.027	0.268	0.500	<b>0.444</b>	0.265
Mean shift	0.219	0.119	<b>0.254</b>	<b>0.232</b>	0.211	0.177	-0.009	0.009
Contrast change	-0.001	0.155	<b>0.585</b>	0.254	0.362	0.252	0.548	<b>0.699</b>
Change of color saturation	0.003	-0.199	0.589	0.169	0.045	<b>0.684</b>	<b>0.631</b>	0.409
Multiplicative Gaussian noise	0.717	0.738	0.704	0.593	0.768	<b>0.849</b>	0.711	<b>0.887</b>
Comfort noise	0.196	0.353	0.318	0.617	0.622	0.406	<b>0.752</b>	<b>0.830</b>
Lossy compression of noisy images	0.609	0.692	0.641	0.712	0.838	0.772	<b>0.860</b>	<b>0.982</b>
Color quantization with dither	0.831	<b>0.908</b>	0.768	0.683	0.896	0.857	0.833	<b>0.901</b>
Chromatic aberrations	0.615	0.570	0.737	0.696	0.753	<b>0.779</b>	0.732	<b>0.768</b>
Sparse sampling and reconstruction	0.807	0.893	0.891	0.865	<b>0.909</b>	0.855	<b>0.902</b>	0.887

TABLE VI

AVERAGE SRCC AND PLCC RESULTS OF INDIVIDUAL DISTORTION TYPE ON LIVE DATABASE. THE TOP TWO RESULTS ARE HIGHLIGHTED IN BOLDFACE.

SRCC	JPEG	JP2K	WN	GB	FF
BRISQUE [27]	0.965	0.929	0.982	<b>0.964</b>	0.828
M3 [32]	0.966	0.930	<b>0.986</b>	0.935	0.902
FRIQUEE [53]	0.947	0.919	0.983	0.937	0.884
CORNIA [54]	0.947	0.924	0.958	0.951	0.921
HOSA [55]	0.954	0.935	0.975	0.954	<b>0.954</b>
dipIQ [61]	<b>0.969</b>	<b>0.956</b>	0.975	0.940	-
DB-CNN [56]	<b>0.972</b>	0.955	0.980	0.935	0.930
FPR	0.962	<b>0.960</b>	<b>0.986</b>	<b>0.959</b>	<b>0.966</b>
PLCC	JPEG	JP2K	WN	GB	FF
BRISQUE [27]	<b>0.971</b>	0.940	0.989	0.965	0.894
M3 [32]	<b>0.977</b>	0.945	<b>0.992</b>	0.947	0.920
FRIQUEE [53]	0.955	0.935	0.991	0.949	0.936
CORNIA [54]	0.962	0.944	0.974	0.961	0.943
HOSA [55]	0.967	0.949	0.983	<b>0.967</b>	<b>0.967</b>
dipIQ [61]	0.980	0.964	0.983	0.948	-
DB-CNN [56]	0.986	<b>0.967</b>	0.988	0.956	0.961
FPR	0.960	<b>0.971</b>	<b>0.991</b>	<b>0.971</b>	<b>0.977</b>

of DIQam-NR are reported from the original paper, and we retrain the HyperIQA by the source codes provided by the authors. All experiments are conducted with one database as training set and the other two databases as testing sets. We present the experimental results in VII, from which we can find the model trained on LIVE (CSIQ) is easier to generalize to CSIQ (LIVE) as similar distortion types introduced by the two databases. However, it is a much more difficult

task to generalize the model trained on CSIQ or LIVE to the TID2013 database, due to these unseen distortion types involved in TID2013 database. Despite this, we can still achieve a high SRCC in the two settings, demonstrating the superior generalization capability of our method.

### C. Ablation Study

In this subsection, to reveal the functionalities of different modules in our proposed method, we perform the ablation study on TID2013 database. To be consistent with the experimental setting on intra-database, 60%, 20%, 20% images in TID2013 are grouped for training, validation and testing sets without content overlapping. Herein, we only report the ablation results by one fixed experimental splitting in Table VIII. In particular, we first ablate the PR and INN modules from our model and retain the Integrity Feature Extractor and GRU based Quality Aggregation modules. The performance drop dramatically due to the fact that no extra constraint be introduced to prevent the overfitting problem. Then we replace the INN module by directly concatenating the learned pseudo reference feature and distortion feature for quality regression, resulting in the second ablation setting. The lower SRCC (0.86 v.s 0.89) reveals that more generalized model can be learned by our INN module. As described before, the triplet loss  $\mathcal{L}_{trip}$  is adopted to learn more discriminative features. In this sense, we ablate the  $\mathcal{L}_{trip}$  in our third experiment. Again, the significant performance dropping reveals that the discriminative PR feature learning is a vital factor for high accuracy quality prediction. Finally, three patch score aggregation modules are compared in Table VIII. The superior performance further demonstrates the effectiveness of our GRU based score aggregation module.

TABLE VII  
SRCC COMPARISON ON DIFFERENT CROSS-DATABASE SETTINGS. THE NUMBERS IN BOLD ARE THE BEST RESULTS.

Training		LIVE		CSIQ		TID2013	
Testing	CSIQ	TID2013	LIVE	TID2013	LIVE	CSIQ	
BRISOU [27]	0.562	0.358	0.847	0.454	0.790	0.590	
M3 [32]	0.621	0.344	0.797	0.328	<b>0.873</b>	0.605	
FRIQUEE [53]	<b>0.722</b>	<b>0.461</b>	0.879	0.463	0.755	0.635	
CORNIA [54]	0.649	0.360	0.853	0.312	0.846	0.672	
HOSA [55]	0.594	0.361	0.773	0.329	0.846	0.612	
DIQaM-NR [15]	0.681	0.392	-	-	-	<b>0.717</b>	
HyperIQA [57]	<b>0.697</b>	<b>0.538</b>	<b>0.905</b>	<b>0.554</b>	0.839	0.543	
Ours	0.620	0.433	<b>0.895</b>	<b>0.522</b>	<b>0.884</b>	<b>0.732</b>	

TABLE VIII  
SRCC PERFORMANCE WITH ABLATION STUDIES PERFORMED ON THE TID2013 DATABASE.

Exp.ID	PR	INN	$\mathcal{L}_{trip}$	Patch Aggregation			SRCC
				Mean	Weighted	GRU	
1	✗	✗	✗			✓	0.670
2	✓	✗	✓			✓	0.859
3	✓	✓	✗			✓	0.772
4	✓	✓	✓	✓			0.869
5	✓	✓	✓		✓		0.848
6	✓	✓	✓			✓	0.887

#### D. Feature Visualization

To better understand the performance of our proposed method, we visualize the quality relevant features  $F^R$ ,  $F^{PR}$ ,  $F^D$  and  $\hat{F}^D$ . More specifically, we first learn two models by our method on TID2013 database and LIVE database, respectively. Then 900 image pairs of each database are randomly sampled from the two databases for testing. For each database, we reduce the feature dimensions of  $F^R$ ,  $F^{PR}$ ,  $F^D$  and  $\hat{F}^D$  to three by T-SNE [62] and the results are visualized in Fig. 3. As shown in Fig. 3, we can observe that the discrepancy of the reference feature  $F^R$  and the pseudo reference feature  $F^{PR}$  is small due to the mutual learning strategy. By contrast, the large discrepancy can be acquired between the pseudo reference feature  $F^{PR}$  and distortion feature  $F^D$  as the triplet loss performed, leading to the better performance.

#### V. CONCLUSIONS

In this paper, we propose a novel NR-IQA method named FPR by restoring the reference information at feature-level. The image quality is evaluated by measuring the discrepancy at the feature-level and the PR feature is inferred based upon the INNs. The mutual learning strategy and triplet loss ensure the learnability and discriminability of PR features. To aggregate the patch-wise quality scores in an image, a GRU based quality aggregation module is further proposed. The superior performance on four synthetic databases demonstrates the effectiveness of our model.

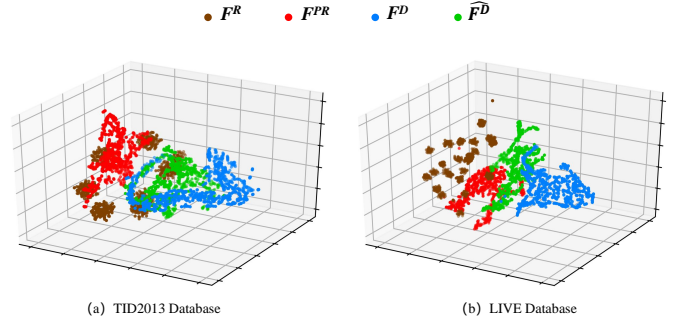


Fig. 3. T-SNE visualization of the features extracted from TID2013 and LIVE databases.

#### REFERENCES

- [1] J. Guo and H. Chao, "Building an end-to-end spatial-temporal convolutional network for video super-resolution," in *Proceedings of the AAAI Conference on Artificial Intelligence*, vol. 31, no. 1, 2017.
- [2] Y. Liu, J. Yan, and W. Ouyang, "Quality aware network for set to set recognition," in *Proceedings of the IEEE Conference on Computer Vision and Pattern Recognition*, 2017, pp. 5790–5799.
- [3] K. Zhang, W. Zuo, S. Gu, and L. Zhang, "Learning deep cnn denoiser prior for image restoration," in *Proceedings of the IEEE conference on computer vision and pattern recognition*, 2017, pp. 3929–3938.
- [4] J. Mannos and D. Sakrison, "The effects of a visual fidelity criterion of the encoding of images," *IEEE transactions on Information Theory*, vol. 20, no. 4, pp. 525–536, 1974.
- [5] Z. Wang, A. C. Bovik, H. R. Sheikh, and E. P. Simoncelli, "Image quality assessment: from error visibility to structural similarity," *IEEE transactions on image processing*, vol. 13, no. 4, pp. 600–612, 2004.
- [6] Z. Wang, E. P. Simoncelli, and A. C. Bovik, "Multiscale structural similarity for image quality assessment," in *The Thirty-Seventh Asilomar Conference on Signals, Systems, and Computers*, 2003, pp. 1398–1402.

*Conference on Signals, Systems & Computers, 2003*, vol. 2. Ieee, 2003, pp. 1398–1402.

[7] L. Zhang, Y. Shen, and H. Li, “Vsi: A visual saliency-induced index for perceptual image quality assessment,” *IEEE Transactions on Image processing*, vol. 23, no. 10, pp. 4270–4281, 2014.

[8] E. C. Larson and D. M. Chandler, “Most apparent distortion: full-reference image quality assessment and the role of strategy,” *Journal of electronic imaging*, vol. 19, no. 1, p. 011006, 2010.

[9] H. R. Sheikh and A. C. Bovik, “Image information and visual quality,” *IEEE Transactions on image processing*, vol. 15, no. 2, pp. 430–444, 2006.

[10] A. K. Moorthy and A. C. Bovik, “Blind image quality assessment: From natural scene statistics to perceptual quality,” *IEEE transactions on Image Processing*, vol. 20, no. 12, pp. 3350–3364, 2011.

[11] M. A. Saad, A. C. Bovik, and C. Charrier, “Blind image quality assessment: A natural scene statistics approach in the dct domain,” *IEEE transactions on Image Processing*, vol. 21, no. 8, pp. 3339–3352, 2012.

[12] W. Hou, X. Gao, D. Tao, and X. Li, “Blind image quality assessment via deep learning,” *IEEE transactions on neural networks and learning systems*, vol. 26, no. 6, pp. 1275–1286, 2014.

[13] L. Kang, P. Ye, Y. Li, and D. Doermann, “Convolutional neural networks for no-reference image quality assessment,” in *Proceedings of the IEEE conference on computer vision and pattern recognition*, 2014, pp. 1733–1740.

[14] J. Kim and S. Lee, “Fully deep blind image quality predictor,” *IEEE Journal of selected topics in signal processing*, vol. 11, no. 1, pp. 206–220, 2016.

[15] S. Bosse, D. Maniry, K.-R. Müller, T. Wiegand, and W. Samek, “Deep neural networks for no-reference and full-reference image quality assessment,” *IEEE Transactions on image processing*, vol. 27, no. 1, pp. 206–219, 2017.

[16] S. Bianco, L. Celona, P. Napoletano, and R. Schettini, “On the use of deep learning for blind image quality assessment,” *Signal, Image and Video Processing*, vol. 12, no. 2, pp. 355–362, 2018.

[17] J. Gu, G. Meng, S. Xiang, and C. Pan, “Blind image quality assessment via learnable attention-based pooling,” *Pattern Recognition*, vol. 91, pp. 332–344, 2019.

[18] J. Fu, H. Wang, and L. Zuo, “Blind image quality assessment for multiply distorted images via convolutional neural networks,” in *2016 IEEE International Conference on Acoustics, Speech and Signal Processing (ICASSP)*. IEEE, 2016, pp. 1075–1079.

[19] J. Kim, A.-D. Nguyen, S. Ahn, C. Luo, and S. Lee, “Multiple level feature-based universal blind image quality assessment model,” in *2018 25th IEEE International Conference on Image Processing (ICIP)*. IEEE, 2018, pp. 291–295.

[20] K. Friston, J. Kilner, and L. Harrison, “A free energy principle for the brain,” *Journal of Physiology-Paris*, vol. 100, no. 1-3, pp. 70–87, 2006.

[21] K. Friston, “The free-energy principle: a unified brain theory?” *Nature reviews neuroscience*, vol. 11, no. 2, pp. 127–138, 2010.

[22] K. Gu, G. Zhai, X. Yang, and W. Zhang, “Using free energy principle for blind image quality assessment,” *IEEE Transactions on Multimedia*, vol. 17, no. 1, pp. 50–63, 2014.

[23] G. Zhai, X. Wu, X. Yang, W. Lin, and W. Zhang, “A psychovisual quality metric in free-energy principle,” *IEEE Transactions on Image Processing*, vol. 21, no. 1, pp. 41–52, 2011.

[24] N. Ponomarenko, L. Jin, O. Ieremeiev, V. Lukin, K. Egiazarian, J. Astola, B. Vozel, K. Chehdi, M. Carli, F. Battisti *et al.*, “Image database tid2013: Peculiarities, results and perspectives,” *Signal Processing: Image Communication*, vol. 30, pp. 57–77, 2015.

[25] H. R. Sheikh, M. F. Sabir, and A. C. Bovik, “A statistical evaluation of recent full reference image quality assessment algorithms,” *IEEE Transactions on image processing*, vol. 15, no. 11, pp. 3440–3451, 2006.

[26] H. Lin, V. Hosu, and D. Saupe, “Kadid-10k: A large-scale artificially distorted iqa database,” in *2019 Eleventh International Conference on Quality of Multimedia Experience (QoMEX)*, 2019.

[27] A. Mittal, A. K. Moorthy, and A. C. Bovik, “No-reference image quality assessment in the spatial domain,” *IEEE Transactions on image processing*, vol. 21, no. 12, pp. 4695–4708, 2012.

[28] P. Ye, J. Kumar, L. Kang, and D. Doermann, “Real-time no-reference image quality assessment based on filter learning,” in *Proceedings of the IEEE Conference on Computer Vision and Pattern Recognition*, 2013, pp. 987–994.

[29] A. K. Moorthy and A. C. Bovik, “A two-step framework for constructing blind image quality indices,” *IEEE Signal processing letters*, vol. 17, no. 5, pp. 513–516, 2010.

[30] H. Tang, N. Joshi, and A. Kapoor, “Learning a blind measure of perceptual image quality,” in *CVPR 2011*. IEEE, 2011, pp. 305–312.

[31] Z. Wang, G. Wu, H. R. Sheikh, E. P. Simoncelli, E.-H. Yang, and A. C. Bovik, “Quality-aware images,” *IEEE transactions on image processing*, vol. 15, no. 6, pp. 1680–1689, 2006.

[32] W. Xue, X. Mou, L. Zhang, A. C. Bovik, and X. Feng, “Blind image quality assessment using joint statistics of gradient magnitude and laplacian features,” *IEEE Transactions on Image Processing*, vol. 23, no. 11, pp. 4850–4862, 2014.

[33] Y. Sun, L. Li, Z. Li, and S. Liu, “Referenceless rate-distortion modeling with learning from bitstream and pixel features,” in *MM '20: The 28th ACM International Conference on Multimedia, Virtual Event / Seattle, WA, USA, October 12–16, 2020*. ACM, 2020, pp. 2481–2489. [Online]. Available: <https://doi.org/10.1145/3394171.3413545>

[34] L. Kang, P. Ye, Y. Li, and D. Doermann, “Simultaneous estimation of image quality and distortion via multi-task convolutional neural networks,” in *2015 IEEE international conference on image processing (ICIP)*. IEEE, 2015, pp. 2791–2795.

[35] W. Zhang, K. Ma, J. Yan, D. Deng, and Z. Wang, “Blind image quality assessment using a deep bilinear convolutional neural network,” *IEEE Transactions on Circuits and Systems for Video Technology*, 2018.

[36] K. Ma, W. Liu, K. Zhang, Z. Duammu, Z. Wang, and W. Zuo, “End-to-end blind image quality assessment using deep neural networks,” *IEEE Transactions on Image Processing*, vol. 27, no. 3, pp. 1202–1213, 2017.

[37] B. Chen, H. Li, H. Fan, and S. Wang, “No-reference screen content image quality assessment with unsupervised domain adaptation,” *IEEE Transactions on Image Processing*, 2021.

[38] X. Liu, J. van de Weijer, and A. D. Bagdanov, “Rankiqa: Learning from rankings for no-reference image quality assessment,” in *Proceedings of the IEEE International Conference on Computer Vision*, 2017, pp. 1040–1049.

[39] Y. Niu, D. Huang, Y. Shi, and X. Ke, “Siamese-network-based learning to rank for no-reference 2d and 3d image quality assessment,” *IEEE Access*, vol. 7, pp. 101 583–101 595, 2019.

[40] Z. Ying, D. Pan, and P. Shi, “Quality difference ranking model for smartphone camera photo quality assessment,” in *2020 IEEE International Conference on Multimedia & Expo Workshops (ICMEW)*. IEEE, 2020, pp. 1–6.

[41] K.-Y. Lin and G. Wang, “Hallucinated-iqa: No-reference image quality assessment via adversarial learning,” in *Proceedings of the IEEE Conference on Computer Vision and Pattern Recognition*, 2018, pp. 732–741.

[42] X. Min, K. Gu, G. Zhai, J. Liu, X. Yang, and C. W. Chen, “Blind quality assessment based on pseudo-reference image,” *IEEE Transactions on Multimedia*, vol. 20, no. 8, pp. 2049–2062, 2017.

[43] Q. Jiang, Z. Peng, G. Yue, H. Li, and F. Shao, “No-reference image contrast evaluation by generating bi-directional pseudo references,” *IEEE Transactions on Industrial Informatics*, 2020.

[44] J. Hu, X. Wang, F. Shao, and Q. Jiang, “Tspr: Deep network-based blind image quality assessment using two-side pseudo reference images,” *Digital Signal Processing*, vol. 106, p. 102849, 2020.

[45] D. He, Y. Xia, T. Qin, L. Wang, N. Yu, T.-Y. Liu, and W.-Y. Ma, “Dual learning for machine translation,” *Advances in neural information processing systems*, vol. 29, pp. 820–828, 2016.

[46] T. Batra and D. Parikh, “Cooperative learning with visual attributes,” *arXiv preprint arXiv:1705.05512*, 2017.

[47] Y. Zhang, T. Xiang, T. M. Hospedales, and H. Lu, “Deep mutual learning,” in *Proceedings of the IEEE Conference on Computer Vision and Pattern Recognition*, 2018, pp. 4320–4328.

[48] X. Lai and Y. Qu, “Adversarial deep mutual learning,” in *2019 IEEE International Conference on Unmanned Systems and Artificial Intelligence (ICUSA)*. IEEE, 2019, pp. 324–329.

[49] F. Schroff, D. Kalenichenko, and J. Philbin, “Facenet: A unified embedding for face recognition and clustering,” in *Proceedings of the IEEE conference on computer vision and pattern recognition*, 2015, pp. 815–823.

[50] H. R. Sheikh, “Image and video quality assessment research at live,” <http://live.ece.utexas.edu/research/quality>, 2003.

[51] A. Paszke, S. Gross, F. Massa, A. Lerer, J. Bradbury, G. Chanan, T. Killeen, Z. Lin, N. Gimelshein, L. Antiga *et al.*, “Pytorch: An imperative style, high-performance deep learning library,” in *Advances in neural information processing systems*, 2019, pp. 8026–8037.

[52] D. P. Kingma and J. Ba, “Adam: A method for stochastic optimization,” *arXiv preprint arXiv:1412.6980*, 2014.

[53] D. Ghadiyaram and A. C. Bovik, “Perceptual quality prediction on authentically distorted images using a bag of features approach,” *Journal of vision*, vol. 17, no. 1, pp. 32–32, 2017.

[54] P. Ye, J. Kumar, L. Kang, and D. Doermann, “Unsupervised feature learning framework for no-reference image quality assessment,” in *2012*

*IEEE conference on computer vision and pattern recognition.* IEEE, 2012, pp. 1098–1105.

- [55] J. Xu, P. Ye, Q. Li, H. Du, Y. Liu, and D. Doermann, “Blind image quality assessment based on high order statistics aggregation,” *IEEE Transactions on Image Processing*, vol. 25, no. 9, pp. 4444–4457, 2016.
- [56] J. Kim, H. Zeng, D. Ghadiyaram, S. Lee, L. Zhang, and A. C. Bovik, “Deep convolutional neural models for picture-quality prediction: Challenges and solutions to data-driven image quality assessment,” *IEEE Signal processing magazine*, vol. 34, no. 6, pp. 130–141, 2017.
- [57] J. Wu, J. Ma, F. Liang, W. Dong, G. Shi, and W. Lin, “End-to-end blind image quality prediction with cascaded deep neural network.” *IEEE Transactions on Image Processing*, vol. 29, pp. 7414–7426, 2020.
- [58] L. Liu, B. Liu, H. Huang, and A. C. Bovik, “No-reference image quality assessment based on spatial and spectral entropies.” *Signal Processing: Image Communication*, vol. 29, no. 8, pp. 856–863, 2014.
- [59] J. Kim, A.-D. Nguyen, and S. Lee, “Deep cnn-based blind image quality predictor,” *IEEE transactions on neural networks and learning systems*, vol. 30, no. 1, pp. 11–24, 2018.
- [60] S. Su, Q. Yan, Y. Zhu, C. Zhang, X. Ge, J. Sun, and Y. Zhang, “Blindly assess image quality in the wild guided by a self-adaptive hyper network,” in *Proceedings of the IEEE/CVF Conference on Computer Vision and Pattern Recognition*, 2020, pp. 3667–3676.
- [61] K. Ma, W. Liu, T. Liu, Z. Wang, and D. Tao, “dipi: Blind image quality assessment by learning-to-rank discriminable image pairs,” *IEEE Transactions on Image Processing*, vol. 26, no. 8, pp. 3951–3964, 2017.
- [62] L. v. d. Maaten and G. Hinton, “Visualizing data using t-sne,” *Journal of machine learning research*, vol. 9, no. Nov, pp. 2579–2605, 2008.